PERFORMANCE ANALYSIS OF ISL'S GUIDED SUPERSONIC PROJECTILE

Pierre Wey

French-German Research Institute of Saint-Louis (ISL)
P.O. Box 70034, 68301 Saint-Louis, France
email : pierre.wey@isl.tm.fr

ISL's Guided Supersonic Projectile is a 30 mm fin-stabilized projectile designed as to increase the effectiveness of air defense guns against maneuvering targets. This multidisciplinary project covers aspects of interior, exterior and terminal ballistics, detonics and on-board electronics. From the early design of the projectile, this paper presents a thorough analysis of the guidance and control process, using both analytical and 6-DOF models. The course correction is based on the control of the angular motion of the projectile which is engaged and stopped using detonator-based impulse thrusters. The analysis shows off the double impulse technique that increases the deflection angle while reducing the loss of velocity. The guidance scheme is an open loop process that consists of a series of quasi-instantaneous trajectory deflections. Without taking into account ballistic and control errors, the correction process can ensure a direct hit at very short range on targets maneuvering up to 9 g's.

PROJECT SUMMARY

ISL's project GSP (Guided Supersonic Projectile) is focused on the guidance and control of medium caliber air defense ammunitions. The early GSP concept and results are described in [1].

The rationale of the project is to increase the effectiveness of air defense gun systems against maneuvering targets such as attack helicopters, UAVs or cruise missiles. In case of evasive motion, the aim error is mainly determined by the inaccurate lead of the moving target (figure 1). This error is typically one to two orders of magnitude greater than the ballistic error.

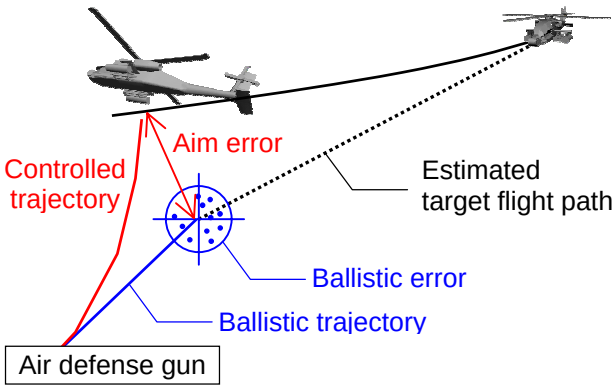

Figure 1. GSP objective: correction of the aim error

The GSP concept is summarized as follows. First of all, the guided projectile is the only new component of the air defense system: the gun, the radar and the fire control device are off-the-shelf components. After firing, the radar continues tracking the target. The flight path of the projectile is then directed toward the updated target location by means of a series of quasi-instantaneous lateral deflections. The deflections result from the control of the angular motion of the projectile. This motion is engaged and stopped using a set of lateral impulse thrusters located at the front part of the projectile as shown in figure 2.

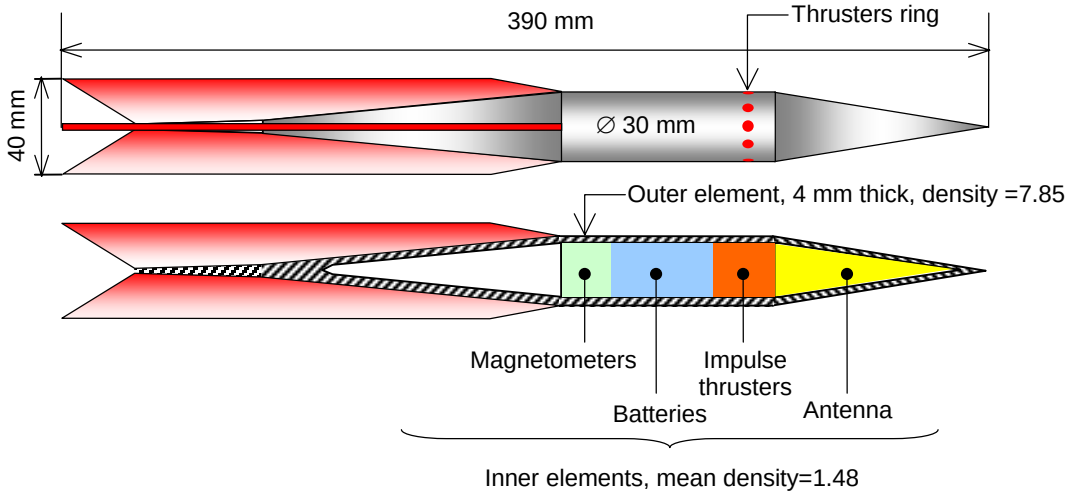

Figure 2. GSP shell

Each impulse thruster is a miniaturized detonator developed at ISL that is fired according to the time series computed by the guidance algorithm running on the ground station. The command which is transmitted from the ground to the projectile consists in the optimal firing time and the related roll angle. This command is received by means of the on-board antenna. The actual firing time is then determined using the real time measurement of the angular attitude performed by the on-board magnetometers [2].

Last but not least, the terminal ballistics performance will benefit from the PELE® architecture which consists in filling the projectile with a low density material [3]. When impacting the target, the projectile is transformed into an effective fragment shower (figure 3a). However, this kill mechanism requires a direct hit. To overcome this problem, another concept can be used: the Active Lateral Penetrator ALP® which consists in a PELE® structure combined with a small quantity of explosive that is triggered before the impact. The resulting spreading of fragments increases the lethal area of the projectile (figure 3b).

Figure 3a. PELE® impact

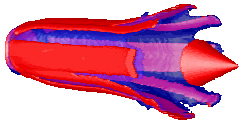

Figure 3b. ALP® concept

BASELINE DATA

In addition to figure 2, table 1 sums up the projectile data based on the current GSP design detailed in [4] (the symbols are listed at the end of the paper). The aerodynamic coefficients have been computed with a CFD code, except for C_{Mq} that is roughly estimated from the Air Force Finner data. The projectile velocity varies from M 3.5 to M 2.5 at 2.6 km range. The initial velocity estimation is based on a muzzle energy of 0.6 MJ (Bofors 40 mm Mk 3 gun) and a sabot mass of 0.140 kg. The roll rate p is required in order to orient the path deflection in any direction. The rate is synchronized with the angular motion so that the projectile makes one half revolution between two successive zeros of the total yaw angle. The roll rate is very slow but higher rates could be considered since the value of the dynamic stability factor S_d indicates that the projectile is always dynamically stable. The detonator-based thrusters have been successfully tested at ISL. They generate an impulse of 2 Ns in 100 μs.

m	0.707 kg
I_x	8.71e-5 kgm^2
I_y	5.04e-3 kgm^2
J	2 Ns
l_{CJ}	2.5 cal

	M 2.5	M 3.5
C_{D0}	0.25	0.19
C_{D2}	13.131	13.131
$C_{L\alpha}$	7.45	7.62
$C_{M\alpha}$	-3.00	-5.39
C_{Mq}	-300	-300

	M 2.5	M 3.5
l_{CP}	0.39 cal	0.69 cal
p	11.9 Hz	22 Hz
T	42.0 ms	22.4 ms
Λ	1190 cal	889 cal
S_d	0.33	0.34

Table 1. GSP data

CONTROL OF THE TRAJECTORY DEFLECTION

Single Impulse

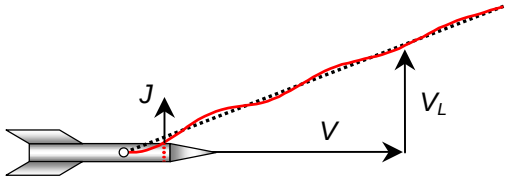

Figure 4. Aerodynamic jump

Let a singular impulse J be engaged at some travel distance s. The impulse vector is normal to the projectile axis and is applied ahead of the center of gravity. This event yields the transverse velocity J/m and triggers the angular oscillation of the projectile. The resulting motion is known as the *aerodynamic jump* [5][6]: the center of mass follows a damped sinusoidal trajectory caused by the action of the lift force, as shown by figure 4. The angular deflection of the flight path can be represented by the velocity V_L imparted by the lift force (V_L is not an

additional velocity). The angular motion of the projectile can be represented using the linearized equation of the complex incidence $\xi = \alpha + i\beta$ as given by McCoy [7]. Neglecting the gravity and the Magnus effects, this equation can be reduced to:

$$\boxed{\xi'' + (H - iP)\xi' - M\xi = 0} \tag{1}$$

where the superscript prime denotes differentiation with respect to the flight path s and:

$$H = \frac{\rho A d}{2m}\left(C_{L\alpha} - C_D - \frac{md^2}{I_y}C_{Mq}\right) \quad (1a) \qquad P = \frac{I_x}{I_y}\frac{pd}{V} \quad (1b) \qquad M = \frac{\rho A d^3}{2I_y}C_{M\alpha} \quad (1c)$$

Considering the impulse as a Dirac function, the initial conditions ξ_0 and ξ'_0 are determined by the impulse vector $J\,e^{i\phi_J}$ as follows:

$$\xi_0 = -\frac{1}{mV}Je^{i\phi_J} \quad (2a) \qquad\qquad \xi'_0 = \frac{l_{CJ}\,d^2}{I_y V}Je^{i\phi_J} \quad (2b)$$

Neglecting ξ_0, the closed-form solution of eq. (1) is then given by:

$$\boxed{\xi = \frac{i\xi'_0}{\phi'_F - \phi'_S}e^{-\frac{H}{2}s}\left(e^{i\phi'_S s} - e^{i\phi'_F s}\right)} \tag{3}$$

where $\phi'_F = \frac{1}{2}\left(P + \sqrt{P^2 - 4M}\right)$ (3a) $\qquad$ $\phi'_S = \frac{1}{2}\left(P - \sqrt{P^2 - 4M}\right)$ (3b)

Using eq. (3), figures 5a, 5b and 5c describe the complete dynamics of the aerodynamic jump. The case is computed at M 3.5 with the data given in table 1, assuming that the impulse is directed upward along the pitch axis (i.e. $\phi_J = 0$). Figure 5a details the motion of the total angle of attack δ, showing off the maximum angle δ_{max} and the distance Λ, which is the distance traveled between two successive minima of $\delta = |\xi|$. Figure 5b presents the pitch-versus-yaw diagram of the complex incidence. The red segment represents the resulting velocity V_L, the orientation of which is denoted by the angle ϕ_{VL}. This angle is due to the gyroscopic effect. Finally, figure 5c details the evolution of the velocities V_L and V_{D2} imparted by the lift and drag forces respectively. Assuming that $C_D = C_{D0} + C_{D2}\delta^2$, V_{D2} is the loss of velocity due to the quadratic yaw-drag coefficient (this loss is zero without oscillations).

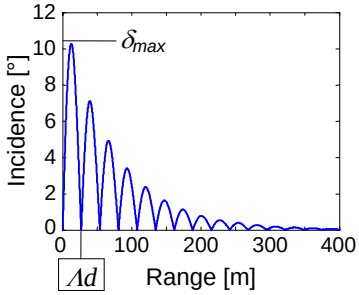

Figure 5a. Total incidence

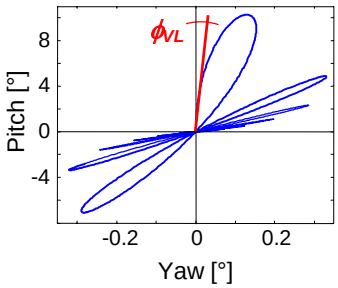

Figure 5b. Pitch vs. Yaw

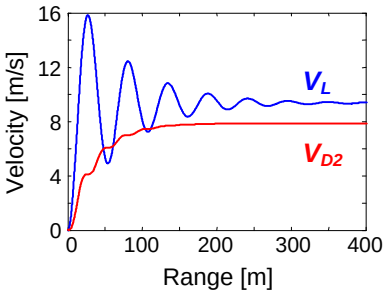

Figure 5c. Imparted velocities

The analytical values of V_L and ϕ_{VL} are computed using the definite integral of ξ, while V_{D2} is computed using the definite integral of ξ^2. Table 2 sums up these results from M 3.5 to M 2.5. The percentage values are the relative difference of the velocities with respect to 6-DOF runs.

	Range [m]	δ_{max} [°]	ϕ_{VL} [°]	V_L [m/s]		V_{D2} [m/s]	
M 3.5	0	10.18	0.13	9.87	+0.5%	7.66	+4.9%
M 3.0	1275	13.30	0.14	13.01	–0.2%	11.75	+4.3%
M 2.5	2661	18.05	0.15	17.14	–1.7%	19.16	+3.8%

Table 2. Single impulse results

The analytical model is very accurate for V_L while it slightly overestimates V_{D2}. However, this overestimation is really negligible when compared to the velocity of the projectile. Therefore, if the minimal velocity is limited to M 2.5, the analytical model is accurate enough to be used in the guidance algorithm.

Repeating the aerodynamic jump using several impulses is the base of the guidance scheme that will be presented hereafter. As a first approach, the total values of V_L and V_{D2} are given by the vector sum of each value resulting from a single impulse. Is there a way to combine these impulses in order to decrease the value of V_{D2}? The answer is yes, thanks to the double impulse technique.

Double Impulse

Let two impulses J_1 and J_2 be engaged at distance s_1 and s_2 respectively. If ξ_1 and ξ_2 are the angular motions due to J_1 and J_2 respectively, the total angular motion is the complex sum $\xi_1+\xi_2$. Suppose that $\phi_{J1} = \phi_{J2} = 0$ and consider three solutions to add the impulses:

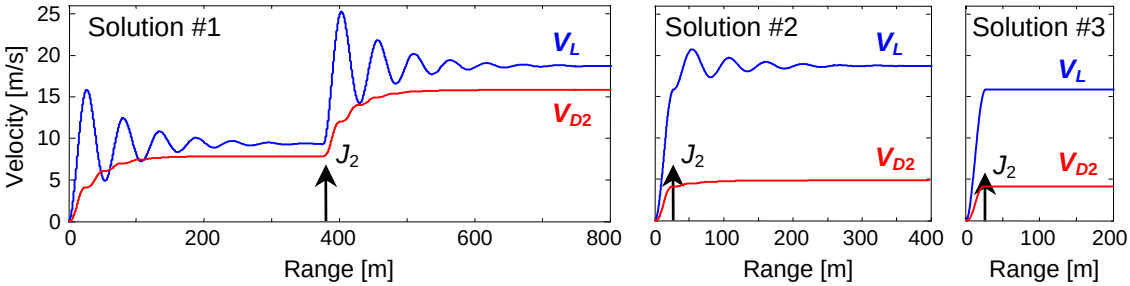

Fig. 6a Fig. 6b Fig. 6c

Figure 6. Adding two impulses

1. $J_2 = J_1$ and $s_2 - s_1 >> \Lambda$: basic solution; the velocities are simply doubled (figure 6a).
2. $J_2 = J_1$ and $s_2 - s_1 = \Lambda$: the angular motion is reduced (but not stopped) by the second impulse which is engaged at the first zero of δ; V_L is still doubled while V_{D2} is reduced by 70% with respect to the first solution (figure 6b).
3. $J_2 = J_1 \, e^{-H/2\Lambda}$ and $s_2 - s_1 = \Lambda$: the second impulse stops the angular motion because it takes into account the damping factor; V_L is multiplied by 1.7 while V_{D2} is reduced by 75% with respect to the first solution (figure 6c).

Figure 7 details all the results as a function of the Mach number. We will investigate here the second solution. As a matter of fact, the third solution is not easy to develop because it requires several types of impulse thrusters. Besides, the firing control is much easier when the thrusters are all identical. Finally, the total deflection velocity vector $\Delta\mathbf{V}$ resulting from the double impulse sequence is defined by the tangential velocity loss $-V_{D2}$ and the normal deflection velocity $2J/m+V_L$. Using the definite integral of $\xi_1+\xi_2$ and neglecting the gyroscopic terms, the deflection velocity is given by:

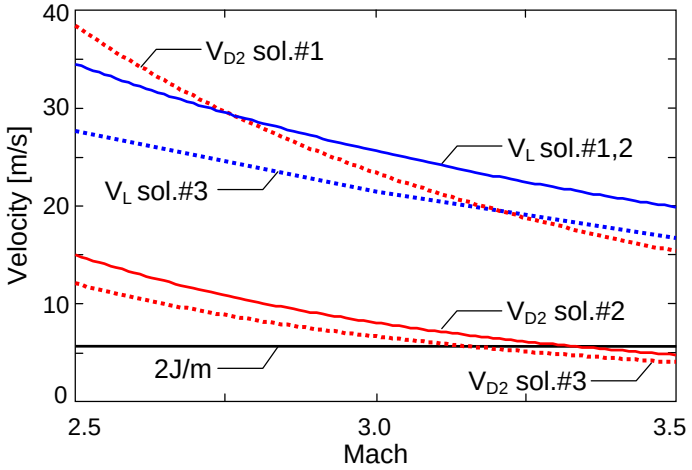

Figure 7. Double impulse results

$$2\frac{J}{m}+V_L = 2\frac{J}{m}\left(1-l_{CJ}\frac{C_{L\alpha}}{C_{M\alpha}}\frac{1}{1-\frac{H^2}{4M}}\right) \tag{4}$$

GUIDANCE MODEL

The guidance scheme is an open loop process that consists of a series of quasi-instantaneous trajectory deflections engaged at time (t_1, t_2, ... t_n). Figure 8 shows the case of a head-on engagement with 3 course corrections. The initial target velocity may range from 100 to 300 m/s. The target acceleration A_T may reach up to 9 g's but is supposed to be fixed during the intercept sequence.

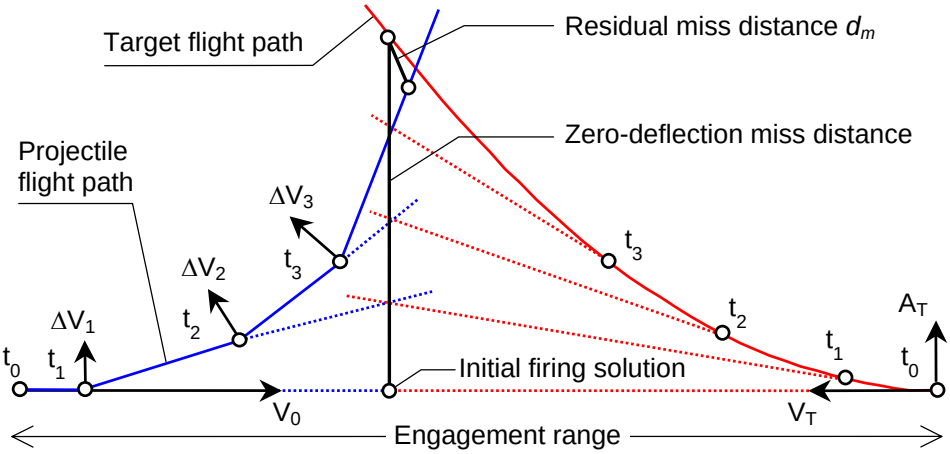

Figure 8. Guidance scheme

After the firing of the projectile, the target and the projectile flight paths are updated according to the same time step which should be about a few milliseconds. The projectile flight path is estimated using a flat-fire ballistics model, while the target motion is estimated using a linear extrapolation of the observed trajectory.

Using this data, the ground-based computer estimates at each time step the miss distance that would result from the projectile course correction. The actual trigger time is the one that minimizes the miss distance, as shown by figure 9. Note that this optimal time should be anticipated in order to minimize the delay required to orient the impulse thruster.

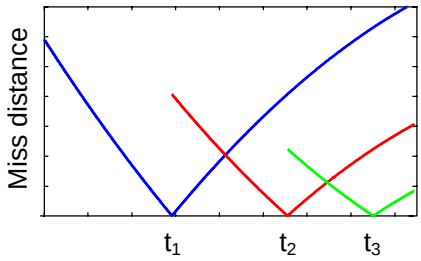

Figure 9. Trigger times

For a given target, the residual miss distance d_m is mainly a function of the number of corrections and of the deflection velocity. It is important to note that the guidance scheme verifies the following property:

$$\lim_{\substack{n \to \infty \\ \Delta V \to 0}} d_m = 0 \tag{5}$$

Thus, the best guidance result is obtained with small but numerous impulses. However, this solution is not relevant because of the integration constraints and also because each control sequence increases the position error of the projectile.

The performance of the guidance and control process is represented by figure 10. The target velocity is set to 100 m/s, its acceleration ranges from 3 to 9 g's and the engagement distance ranges from 1000 to 3000 m (the minimal projectile velocity is thus limited to M 2.5).

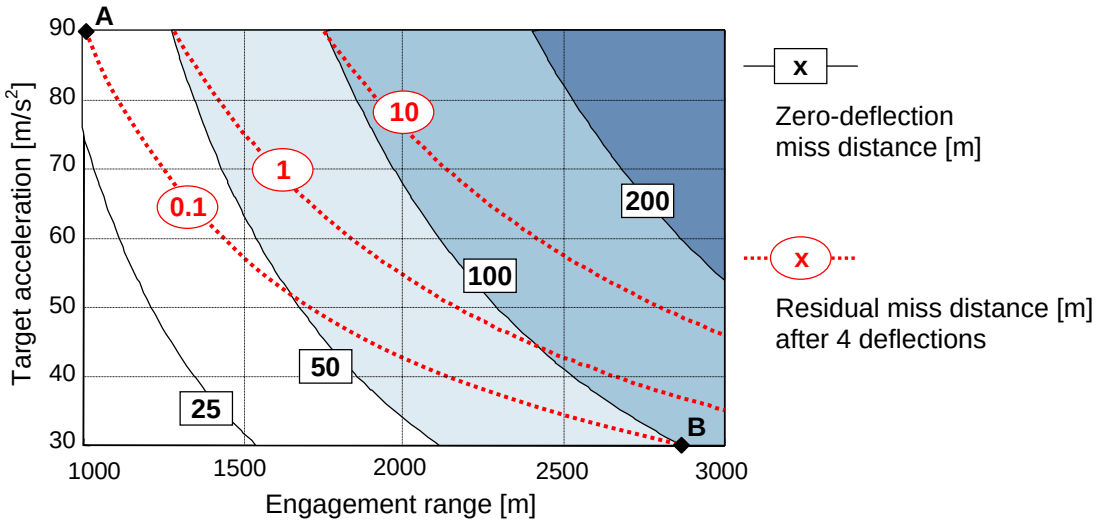

Figure 10. Performance of the guidance and control process

Thanks to 4 deflections (i.e. 8 impulses), the course correction can theoretically ensure a direct hit at very short range, as shown by the 0.1 m contour line. Considering the 1 m contour line, it can be seen that the reduction factor of the miss distance ranges from 50 to more than 100. These results prove the relevance and the consistency of the guidance and control process. However, this process does not correct the initial ballistic error since the projectile flight path is only estimated. Besides, as mentioned above, it generates additional errors. Table 3 gives the miss distance computed at points A and B (figure 10) due to the error on three main parameters. The full error analysis will therefore be the next step of the GSP performance analysis.

	Initial velocity		Deflection velocity		Trigger time	
	-5%	+5%	-5%	+5%	-10 ms	+10 ms
A	3.2	2.6	1.5	1.4	1.0	1.1
B	12.8	8.7	4.8	5.0	1.1	1.2

Table 3. Error analysis (residual miss distance in m)

LIST OF SYMBOLS

A	projectile reference area [m^2]	p	projectile axial spin [s^{-1}]
A_T	target acceleration [ms^{-2}]	s	distance along flight path [cal]
C_{D0}	zero-yaw drag coefficient	S_d	dynamic stability factor
C_{D2}	quadratic-yaw drag coefficient $C_D = C_{D0} + C_{D2}\delta^2$	V	projectile velocity [ms^{-1}]
$C_{L\alpha}$	lift force coefficient derivative	V_{D2}	loss of velocity due to quadratic-yaw drag [ms^{-1}]
$C_{M\alpha}$	pitching moment coefficient derivative	V_L	velocity imparted by lift force [ms^{-1}]
$C_{N\alpha}$	normal force coefficient derivative	V_T	target velocity [ms^{-1}]
d	projectile reference caliber [m]	α	pitch angle
d_m	residual miss distance [m]	β	yaw angle
l_{CP}	positive distance from CG to center of pressure (static margin) [cal]	ΔV	total deflection velocity [ms^{-1}]
l_{CJ}	positive distance from CG to location of applied impulse [cal]	δ	total yaw angle for small angles: $\delta = (\alpha^2 + \beta^2)^{1/2}$
m	projectile mass [kg]	Λ	distance between two successive minima of the total yaw angle [cal]
n	number of flight path deflections	ρ	air density [kgm^{-3}]
I_x	projectile axial moment of inertia [kgm^2]	ξ	complex incidence $\xi = \alpha + i\beta = \delta e^{i\Phi}$
I_y	projectile transverse moment of inertia [kgm^2]	ϕ_J	orientation of vector **J**
J	impulse [Ns]	ϕ_{VL}	orientation of vector $\mathbf{V}_L$

REFERENCES

[1] P. Wey, C. Berner, E. Sommer, V. Fleck, H. Moulard, Theoretical Design for a Guided Supersonic Projectile, *22nd International Symposium on Ballistics* (2005)

[2] V. Fleck, R. Meyer, E. Sommer, Onboard Measurements of the Motion of Projectiles with Accelerometers and Magnetometers, *21st International Symposium on Ballistics* (2004)

[3] G. Paulus, P.-Y. Chanteret, E. Wollmann, PELE: A New Penetrator Concept for the Generation of Lateral Effects, *21st International Symposium on Ballistics* (2004)

[4] C. Berner, E. Sommer, V. Schirm, P. Wey, Preliminary Design for ISL's Guided Supersonic Projectile, *23rd International Symposium on Ballistics* (2007)

[5] R.L. McCoy *et al*., Linearized Swerving Motion of Rotationally Symmetric Projectiles, in *Modern Exterior Ballistics: The Launch and Flight Dynamics of Symmetric Projectiles*, 240-251

[6] G.R. Cooper, Projectile Aerodynamic Jump Due to Lateral Impulsives, ARL -TR-3087 (2003)

[7] R.L. McCoy *et al* , Linearized Pitching and Yawing Motion of Rotationally Symmetric Projectiles, in *Modern Exterior Ballistics: The Launch and Flight Dynamics of Symmetric Projectiles*, 221-239